SAFETY ANALYSIS OF THE ACCELERATOR-DRIVEN TEST FACILITY

X. Cheng,[1] **J.E. Cahalan**[2] and **P.J. Finck**[2]
1. Forschungszentrum Karlsruhe, Postfach 3640, D-76021 Karlsruhe, Germany
Email: xu.cheng@iket.fzk.de
2. Argonne National Laboratory, 9700 South Cass Avenue, Argonne, IL 60439, USA

Abstract

Analysis of the dynamic behaviour of ADTF has been carried out in the framework of a bilateral collaboration between the Forschungszentrum Karlsruhe and Argonne National Laboratory (ANL). For this purpose, SAS4A the safety analysis code was applied to five systems with different types of fuel and coolant.

In sodium-cooled systems, transient behaviour in the unprotected loss-of-flow scenario shows the least favourable safety performance. As long as the external source is present, loss of coolant flow will lead to an overheating of coolant, cladding and fuel. Coolant boiling, cladding failure and molten fuel injection take place several seconds after the coast-down of the pump. Compared to metallic fuel, oxide fuel does not improve the dynamic behaviour significantly, yielding only a delay of the onset of pin failure by a few seconds. Safety measures must be designed for switching off the proton beam.

In systems cooled with lead-bismuth eutectic (LBE), the buoyancy effect is much stronger. Due to the high boiling point of LBE, coolant boiling and, subsequently, flow oscillation in fuel assemblies can be avoided. By proper design of the heat removal system, natural convection can provide sufficient cooling of the reactor core to maintain the integrity of the fuel pins.

1. Introduction

In the Advanced Accelerator Application Program of the US Department of Energy, an Accelerator-driven Test Facility (ADTF) with a thermal power of 100 MW has been proposed. One of the main objectives of the ADTF is the demonstration of the feasibility of the accelerator-based transmutation of nuclear waste. Analysis of the dynamic behaviour of the ADTF has been carried out in the framework of a bilateral collaboration between the Forschungszentrum Karlsruhe and Argonne National Laboratory (ANL). For this purpose, the ANL safety analysis code SAS4A was used. The main purpose of this work is to study the dynamic behaviour of different system configurations of the sub-critical test facility. Thus, five systems with different types of fuel and coolant have been taken into consideration. Analysis of various transient scenarios was carried out, i.e. double external source, protected loss-of-flow, unprotected loss-of-flow and unprotected loss-of-heat sink.

This paper summarises the results obtained so far. The effect of different types of fuel and coolant on the dynamic behaviour of the test facility is analysed.

2. System configurations

At the pre-conceptual design phase, many options are still open related to the design of the reactor core as well as the primary loop. In general, the existing technology gained at EBR-II has been applied to ADTF as far as possible. [1] Some components of the primary loop will be the same as that available at EBR-II.

Figure 1. **Scheme of the primary system**

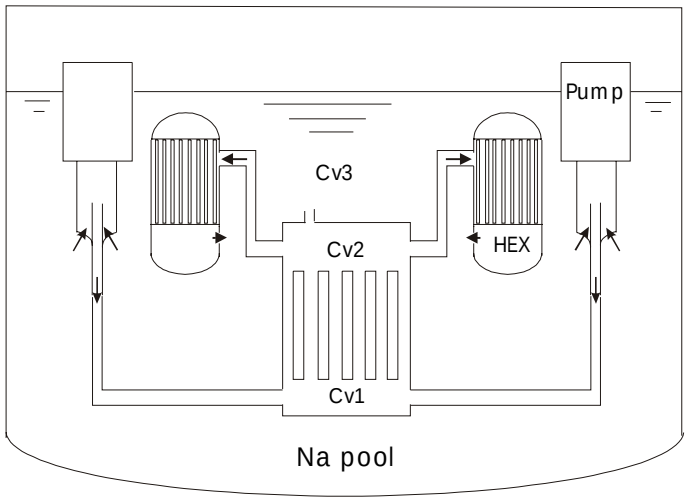

The entire primary loop is considered in the SAS calculation and schematically shown in Figure 1. The intermediate loop is neglected using a pre-defined temperature drop over the heat exchangers as a boundary condition. Due to the higher thermal power of ADTF (100 MW) compared to EBR-II (62 MW [2]), two loops are proposed. Each loop contains one intermediate heat exchanger and one pump. For the present analysis, the technical specification of the heat exchanger and the pump is the same as that used at EBR-II. The entire primary system is divided into 10 liquid segments, i.e. channels, 4 bypasses, 2 hot legs, 2 cold legs and 1 leakage path.

In this study, five system configurations have been taken into consideration with different types of fuel and coolant. Table 1 summarises some specifications of configurations studied. The name of the configurations consists of two parts. The first part indicates the type of fuel, i.e. MET for metallic fuel and OXI for oxide fuel. The second part shows the type of coolant, i.e. NA for sodium cooled systems and LBE for lead-bismuth cooled systems.

Table 1. **Specifications of different configurations**

System configurations	**Reference**	**MET-NA**	**OXI-NA**	**MET-LBE**	**OXI-LBE**
Fuel	Metallic	Metallic	Oxide	Metallic	Oxide
Coolant	Sodium	Sodium	Sodium	LBE	LBE
Sub-assembly configuration	EBR-2	FFTF	FFTF	ATW/ FFTF	ATW/ FFTF
No. of SAs	120	64	64	64	64
No. of pins in one SA	61	217	217	217	217
Pin diameter [mm]	5.842	5.842	5.842	5.80	5.80
Pin pitch [mm]	6.909	7.264	7.264	9.80	9.80
Clad thickness [mm]	0.457	0.381	0.381	0.70	0.70
Gap size [mm]	0.330	0.100	0.070	0.20	0.050
Fuel length [mm]	342.9	917.9	917.9	917.9	917.9
Power density [W/cm]	400	80	80	80	80
Mass flow rate [kg/s]	798	798	798	7103	7103
Spallation target	W-Na	W-Na	W-Na	LBE	LBE

In the so-called reference design, the fuel, the coolant and the sub-assembly configuration are the same as in EBR-II. However, the linear power in the reference design is much higher than in EBR-II. In the OXI-NA configuration, the fuel assembly of FFTF [3] is used. In the MET-NA configuration, the fuel assembly design is taken from FFTF. Instead of oxide fuel, metallic fuel is used. In the sodium cooled systems, a sodium cooled tungsten target (W-Na) was proposed. In the case of metallic fuel, the gap between the cladding and the fuel is filled with liquid metal. The gap size is also larger than in the oxide fuel systems, where the gap is filled with gas. In an LBE cooled system, a wide fuel lattice is used to increase the coolant flow area, and thus to reduce the coolant velocity. This is required to minimise the corrosion and erosion problem. The fuel assembly configuration is similar to that considered in the design of a LBE-cooled ATW. [5] The geometric parameters of the fuel pin are assumed to be the same as those of the FFTF fuel pin. [3] In both of the LBE-cooled systems, an LBE spallation target is proposed.

The thermal power released in the sub-critical multiplier and in the spallation target are 100 MW and 3.5 MW, respectively. Assuming that the average temperature rise of the coolant over the reactor core is 100 C, the required mass flow is 798 kg/s for the sodium cooled configurations and 7 103 kg/s for the LBE-cooled configurations. About 5% of the total coolant flows through the spallation target. Furthermore, it is assumed that about 10% of the total mass flow goes through the buffer zone and the reflector region.

Neutron-physical analysis was carried out for both the reference configuration and the OXI-NA configuration. [4] Assumptions have been made to generate the complete neutron-physical data required for the SAS4A calculation. Table 2 summarises the reactivity feedback data for different configurations. The initial k-effective is 0.971. [4] The radial power distribution for the reference

configuration and the OXI-NA configuration is taken from [4]. It is assumed that the radial power distribution in the MET-NA, MET-LBE and OXI-LBE configurations are the same as in the OXI-NA configuration. The axial power distribution was taken from [6], where it was originally derived for a core configuration similar to the reference proposal.

Table 2. **Reactivity feedback data for different configurations**

Configuration	**Doppler** [pcm/C]	**Void** [pcm/kg]	**Fuel worth** [pcm/kg]	**Cladding worth** [pcm/kg]
Reference	-70	-49.5	69.6	-3.40
MET-NA	-70	-5.04	10.3	-0.95
OXI-NA	-422	-5.04	15.2	-0.95
MET-LBE	-70	-0.175	10.3	-0.95
OXI-LBE	-422	-0.175	15.2	-0.95

3. Results and discussion

Five different cases have been analysed in this study, i.e. steady state (SS), doubled external source (DES), unprotected loss of flow (ULOF), unprotected loss of heat sink (ULOHS) and protected loss-of-flow (LOF). Except for the reactor power and the feedback reactivity, which are average values over the entire reactor core, all other parameters presented in this section are related to the channel with the highest power density. If it is not explicitly indicated, the axial location is the upper end of the fuel pin.

3.1 Steady state condition

Table 3 summarises the pressure loss in different parts of the primary loop for different configurations.

Table 3. **Pressure loss [bar] in different parts of the primary system**

	Reference	**MET-NA**	**OXI-NA**	**MET-LBE**	**OXI-LBE**
ΔP_f – core	1.876	1.425	1.425	0.493	0.493
ΔP_f – hot leg	0.568	0.245	0.245	0.439	0.439
ΔP_f – cold leg	1.050	0.129	0.129	0.150	0.150
ΔP_f – loop	3.494	1.799	1.799	1.082	1.082

The reference configuration has the largest pressure loss, although the length of the sub-assembly is only 50% of the other configurations. This is mainly due to a higher coolant velocity, which is 6.4 m/s in the reference configuration compared to 3.9 m/s in the other sodium cooled configurations. The total pressure loss in the reference configuration is about 3.5 bar, of which 1.9 bar occurs over the reactor core. Due to the wider lattice structure, the pressure loss over the LBE-cooled reactor core is much lower than that over the sodium-cooled cores. Compared to the reference configuration, the piping system of the other configurations is simplified, so that the pressure loss in the primary loop (except the reactor core) is reduced significantly. Although the pressure loss in the primary piping system is somewhat higher, the total pressure loss of the primary loop in the LBE-cooled systems is only about one half of that in a Na-cooled system.

Figure 2 shows the temperature distribution of the fuel, the cladding and the coolant in different configurations.

Figure 2. **Temperature distribution of the fuel, the cladding and the coolant in different configurations**

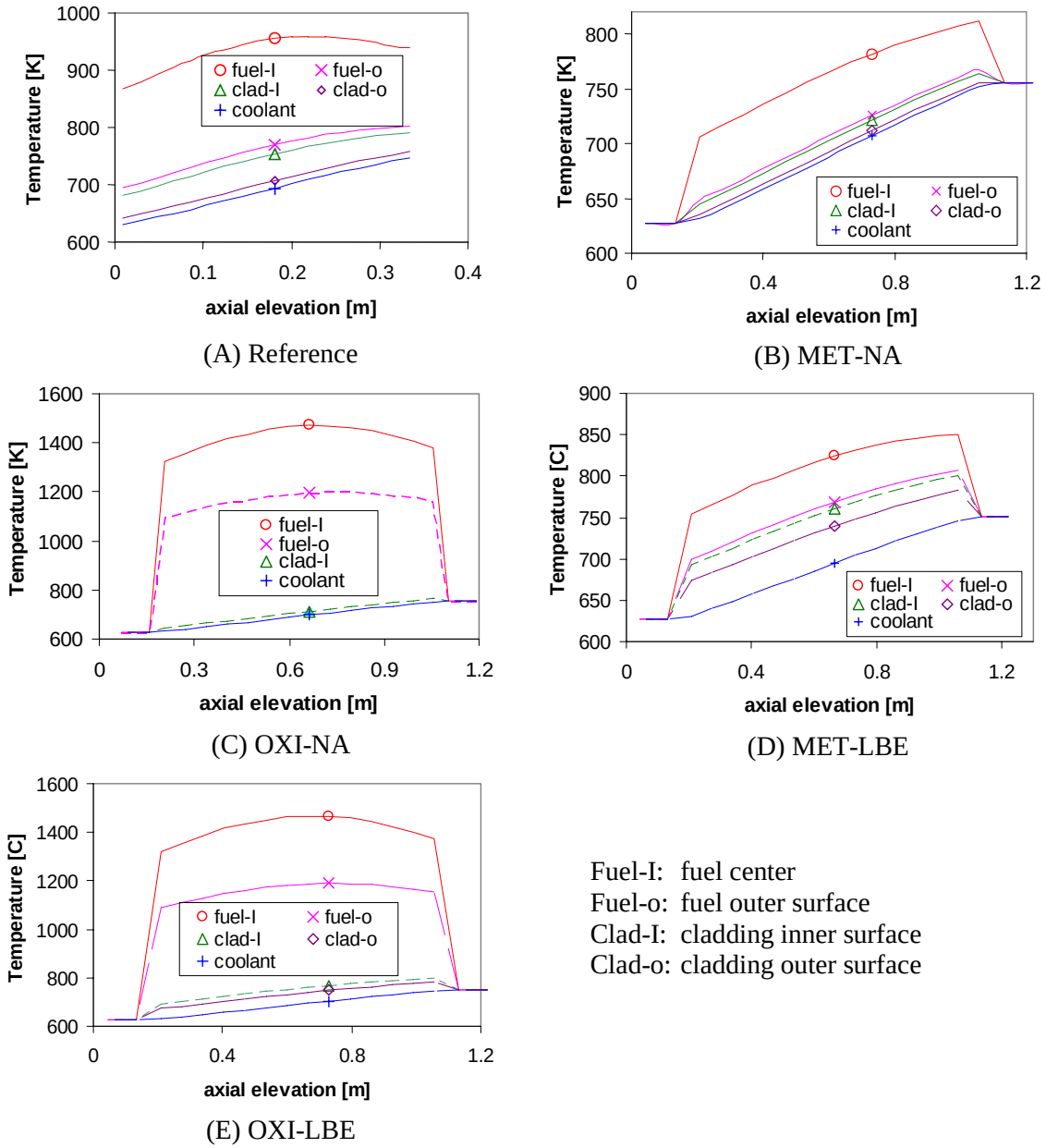

Fuel-I: fuel center
Fuel-o: fuel outer surface
Clad-I: cladding inner surface
Clad-o: cladding outer surface

In the systems with metallic fuel, the fuel temperature is significantly lower than in a system with oxide fuel. This is due to the higher thermal conductivity and the lower temperature drop across the gap between the fuel and the cladding in metallic fuel In the case with oxide fuel, the temperature drop across the gap is as high as 500°C. The profile of the fuel temperature is significantly different. In a metallic fuel system, the maximum fuel temperature is located close to the upper end of the fuel pin, whereas in an oxide fuel configuration, the temperature peak is found in the central region of the fuel

pin. The maximum fuel temperature is about 1 500 K in oxide fuel, which is far below the melting point (≈3 000 K). In the reference configuration, the maximum fuel temperature is about 960 K, much higher than in the other metallic fuel configurations (≈800 K).

Because of the higher linear power density, the temperature drop across the cladding in the reference configuration is much higher than in the other configurations. In the sodium-cooled configurations, the heat transfer from the cladding to the coolant is much more efficient than in the LBE-cooled configurations. This leads to a much smaller temperature drop across the cladding surface.

3.2 Double external source transient (DES)

Variation of the proton beam power is one of the options to compensate the burn-up reactivity swing. In this case, the maximum available beam power will be higher than the required beam power at the beginning of the fuel cycle. Design of the safety system must take into consideration the case with an enhanced external source. In the transient analysed in this sub-section, the external source is doubled spontaneously. All the other operating parameters are kept unchanged. Figure 3 shows the behaviour of the reference configuration under the double external source transient. The reactor power increases rapidly by about 85%. This leads to a rise of the fuel temperature of about 300 K. The negative feedback reactivity keeps the power rise below the factor 2. After the first several seconds, the temperatures of fuel, cladding and coolant increase continuously, due to the warm-up of the sodium pool. It has been assumed that the temperature drop over the intermediate heat exchangers is kept unchanged. During the transient, the mass flow rate is hardly changed. Therefore, the amount of heat removed by the intermediate heat exchanger is almost the same. The increase in the reactor power leads to a warm-up of the sodium pool. The effective pool volume is 180 m^3. Assuming that the over-power is 85% of the nominal power, i.e. 85 MW, the rate of the pool temperature rise is 0.40 k/s. This agrees well with the results obtained with the SAS4A code. The boiling point of sodium is about 1 300 K and will be reached in about 20 minutes. In about 400 s the fuel temperature reaches the solidus temperature and fuel melting begins. At the time point t=1 000 s, the local fuel molten fraction is as high as 35%. Due to the formation of eutectic alloys between the metallic fuel and steel, the local cladding thickness is reduced. Due to the reduction in the cladding thickness, cladding failure in channel 1 occurs at t=690 s. As recognised in Figure 3E, at the time point t=1 000s, cladding failure occurs over the region from z=0.18 m to the upper end of the fuel pin.

In the other four systems, similar behaviour of the reactor power and the channel mass flow rate is found. Due to the lower linear power compared to the reference design (see Table 1), the increase in the fuel temperature, the cladding temperature and the coolant temperature is much milder. This leads to a delayed occurrence of pin failure.

Figure 3. **Transient behaviour of the reference configuration under double external source conditions**

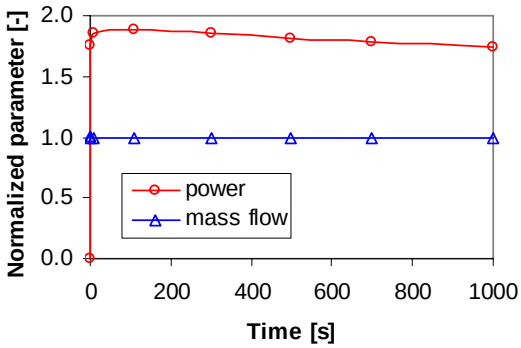

(A) Normalised power and mass flow

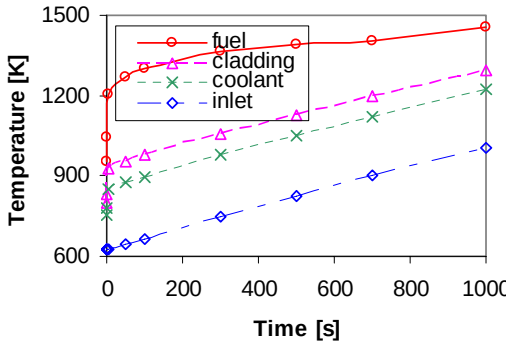

(B) Temperatures

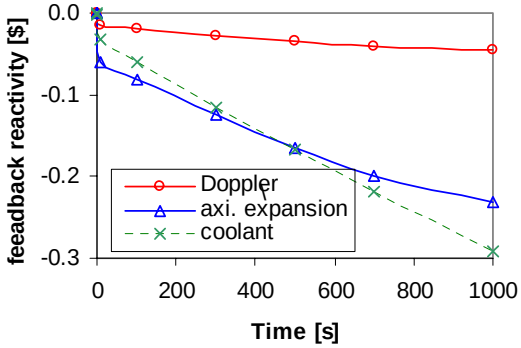

(C) Feedback reactivity

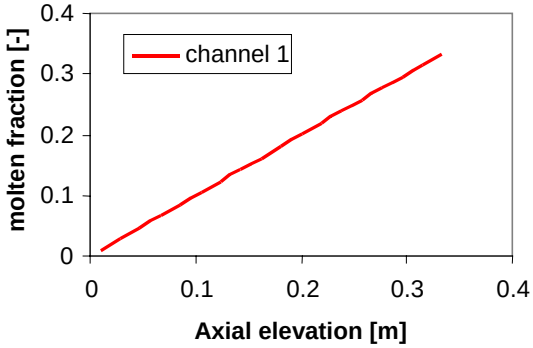

(D) Molten fuel fraction at t = 1 000 s

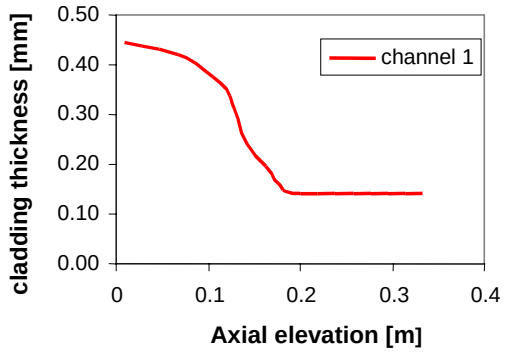

(E) Cladding thickness at t = 1 000 s

3.3 Unprotected loss of heat sink

In this case, the temperature drop over the heat exchanger is assumed to decrease spontaneously from 100% down to 0%. The heat removal via the heat exchanger is completely eliminated. Figure 4

shows the behaviour of the reference configuration under ULOHS conditions. The temperature of the fuel, the cladding and the coolant increases approximately in the same rate as the sodium pool temperature. The dynamic behaviour in this case is similar to the case with a doubled external source, except for the first few seconds.

Figure 4. **Transient behaviour of the reference configuration under the unprotected LOHS condition**

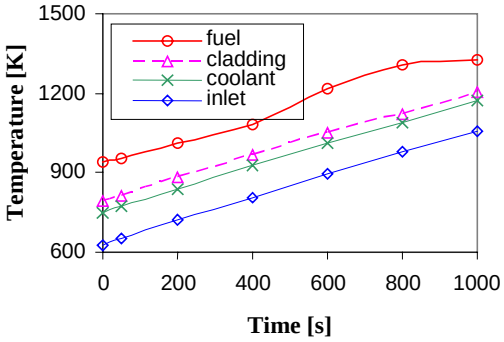

Figure 5. **Coast-down curve of the primary pump**

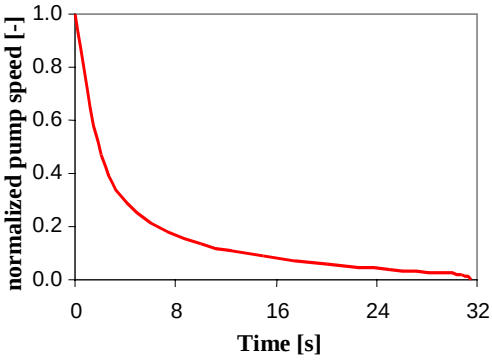

3.4 Unprotected loss of flow

For this analysis, it is assumed that the power supply (from the generators) to both primary pumps is broken at the time point t=0. The coast-down behaviour of both pumps is taken from [6], as illustrated in Figure 5. The pump speed goes down to zero in about 30 s.

3.4.1 Sodium-cooled systems

Figure 6 shows the behaviour of the reference configuration under the ULOF condition. At the beginning, the mass flow through both the channel and the target is consistent with the pump coast-down curve. During the coast-down of the pump, the temperature of fuel, cladding and coolant (at the elevation of the upper end of the fuel pin) increases rapidly. After the onset of boiling, the coolant flow rate through the boiling channel decreases rapidly. Flow oscillation occurs. The flow rate through the target increases and the normalised flow rate is well above the pump coast down curve. This keeps the coolant temperature in the target well below the boiling point. Obviously, sodium boiling leads to a reduction in the heat transfer from the cladding to the coolant. The cladding temperature increases sharply. After a short delay, a sharp increase in the fuel temperature occurs. Due to the eutectic formation of the metallic fuel with the cladding material, cladding is dissolved and becomes thinner. For cladding pressurised by released fission gas, cladding failure occurs prior to the cladding temperature reaching its melting point, due to the hoop stress in the thinned cladding exceeding the ultimate tensile strength. First injection of the molten fuel into the coolant channel happens at a time point of 9.80 s.

The coolant boiling causes a large negative feedback reactivity, which leads to a strong reduction in the reactor power. The molten fuel injection causes fuel relocation, and subsequently, leads to a negative feedback reactivity. The Doppler feedback reactivity is small compared to the other reactivity feedback terms.

In the MET-NA system, the behaviour is similar to that of the reference configuration, except delayed onset of boiling (12.6 s) and molten fuel injection (17.7 s).

Figure 6. **Behaviour of the reference configuration under ULOF conditions**

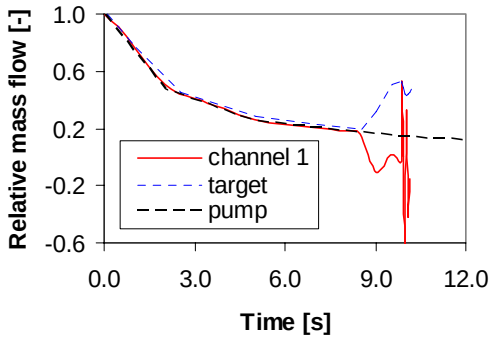

(A) Normalised mass flow

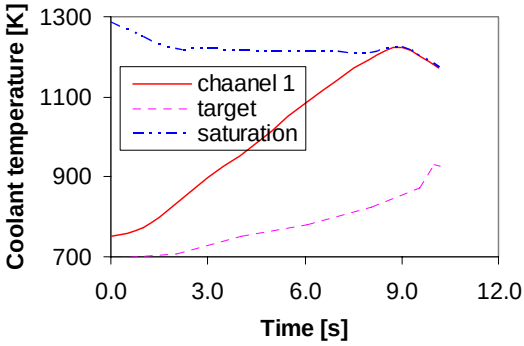

(B) Coolant temperature

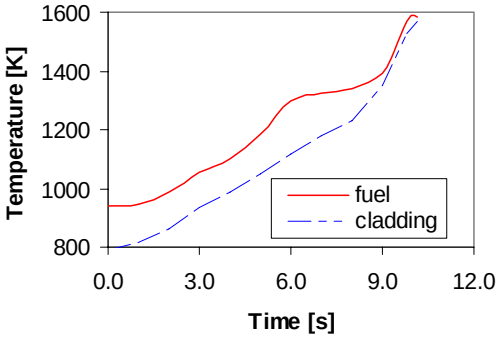

(C) Fuel/cladding temperature

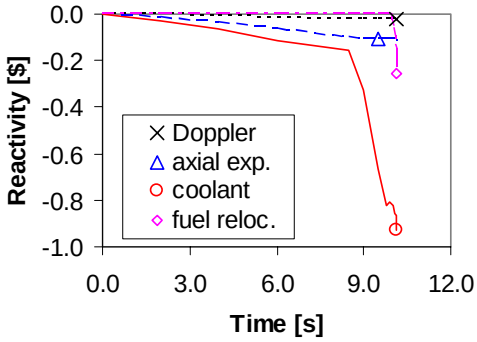

(D) Feedback reactivity

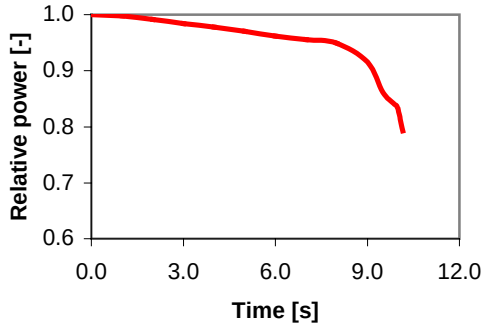

(E) Normalised reactor power

3.4.2 LBE-cooled systems

Figure 7 shows the behaviour of the MET-LBE configuration under ULOF conditions. It is seen that the normalised flow rate through the channels is far above the pump coast-down curve due to enhancement of the buoyancy-driven natural convection as the coolant hot leg temperature rises. In about 30 s, a new steady state is established under natural convection conditions. The coolant flow rate is as high as 35% of the nominal value. The coolant temperature is about 1 000 K, well below the boiling point. The cladding temperature and the fuel temperature are low, so that cladding failure or fuel melt-down is avoided. The feedback reactivity is low, because the temperature change is small,

and there is no phase change of the coolant, the cladding and the fuel. Similar behaviour has been obtained for another LBE cooled configuration (OXI-LBE). Obviously, the LBE cooled systems with a wider lattice can cope with the ULOF transient without serious safety concern.

Figure 7. **Transient behaviour of the MET-LBE configuration under ULOF conditions**

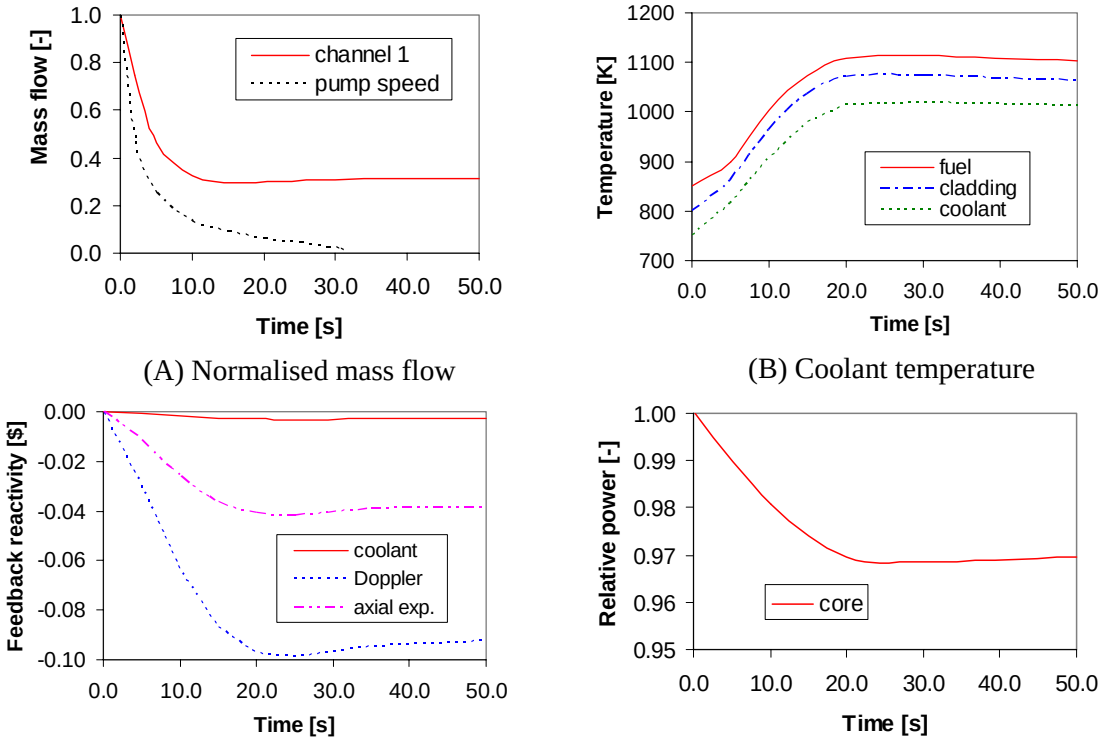

(A) Normalised mass flow

(B) Coolant temperature

(C) Feedback reactivity

(D) Normalised reactor power

This significant merit of a LBE-cooled system is mainly led back to the thermal-physical properties of LBE and the specific design of the wider lattice, which enables the operation under natural convection conditions. Using a simplified 1-D approach, the mass flux G and the temperature rise ΔT over the reactor core under natural convection conditions is given by the following equations:

$$\frac{G}{G_0} = \left\{ \frac{\Delta P_{g0} \cdot Q}{\Delta P_{f0} \cdot Q_0} \right\}^{1/3} \tag{1}$$

$$\frac{\Delta T}{\Delta T_0} = \left\{ \frac{\Delta P_{f0} \cdot Q^2}{\Delta P_{g0} \cdot Q_0^2} \right\}^{1/3} \tag{2}$$

Here Q, ΔP_f and ΔP_g are heat power, friction pressure drop and gravitational pressure head, respectively. The subscript 'o' stands for the normal operating conditions. In a LBE cooled system, the gravitational pressure head ΔP_{g0} is about 4 times greater than in a Na-cooled system. Due to the wider lattice design and low coolant flow velocity the pressure loss is lower in an LBE-cooled system. As indicated in Table 3, the pressure loss in a LBE-cooled system is about one half of a Na-cooled system. This gives a much higher mass flux and a much lower coolant temperature rise in a LBE-cooled system under natural convection conditions.

3.4 Protected loss of flow (P-LoF)

As mentioned above, serious safety concern might arise in a Na-cooled system under the ULOF transient. Therefore, safety system has to be designed to switch off the external source. In the past, passive measures have been analysed to switch off or to damp the proton beam out of the reactor core. [8] The dynamic behaviour of different systems under protected LOF conditions has been analysed in this study. The results presented in this section are obtained under the assumption that the external source is reduced linearly from 100% to 0% in the time range from 5 s to 10 s after the beginning of the pump coast-down.

Figure 8. **Behaviour of the reference system under protected LOF conditions**

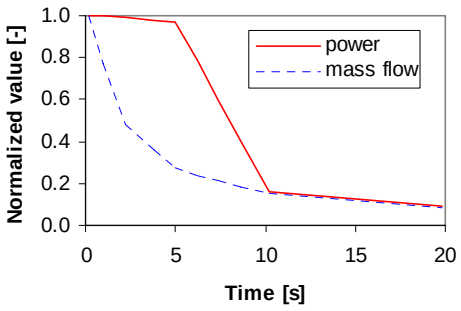

(A) Normalised power and mass flow over a short time scale

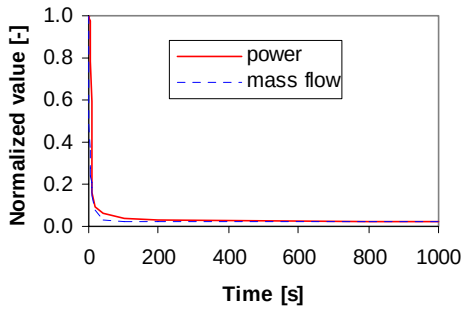

(B) Normalised power and mass flow over a large time scale

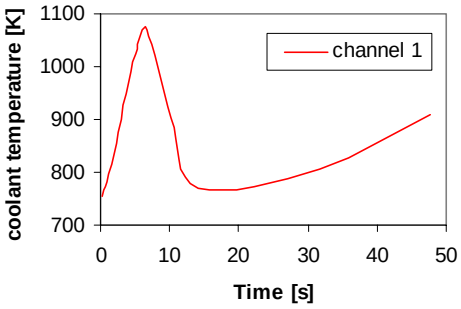

(C) Coolant temperature over a short time scale

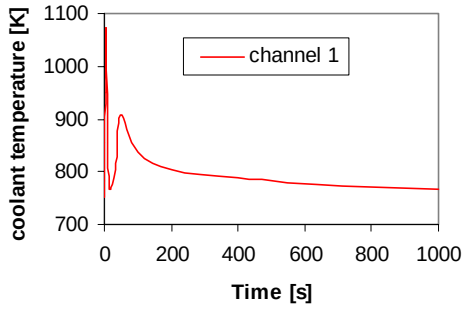

(D) Coolant temperature over a large time scale

3.5.1 Sodium-cooled systems

Figure 8 shows the transient behaviour of the reference system under protected LOF conditions. The reactor power is reduced from 98% at the time point t=5 s down to about 15% at the time point t=10 s. After then the normalised reactor power and the mass flow rate decline with almost the same rate. The coolant temperature reaches its maximum value (1 070 K) in about 9 s, and decreases again due to the reduction in the reactor power. During the entire transient, the coolant temperature is well below the boiling point. After several seconds, a new relationship between the reactor power, the mass flow rate and the coolant temperature is established under natural convection conditions.

3.5.2 LBE-cooled systems

Figure 9 shows the dynamic behaviour of the MET-LBE configuration under unprotected LOF condition. Compared to the Na-cooled systems, the normalised mass flow rate in a LBE-cooled reactor

is much higher. At the time point t=1 000 s, the mass flow rate is still about 10% of the nominal value, although the reactor power is reduced to about 2% of the nominal value. This high mass flow rate would keep the coolant temperature, the cladding temperature and the fuel temperature at a much lower level.

Figure 9. **Transient behaviour of the MET-LBE system under protected LOF conditions**

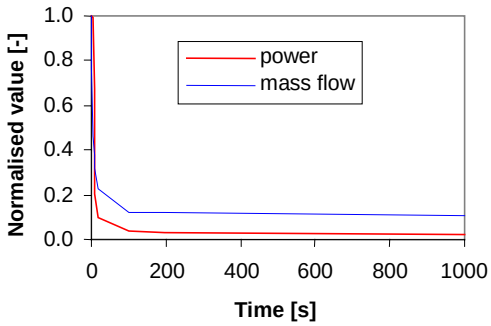

4. Summary

Analysis of the dynamic behaviour of the ADTF facility has been carried out using the SAS4A code. The main purpose of this study is to provide basic knowledge about the safety features of the ADTF facility. Five system configurations have been considered with different types of fuel and coolant. The dynamic behaviour of these systems was investigated under the transient scenarios of doubled external source, protected loss of flow, unprotected loss of flow and unprotected loss of heat sink. The results achieved so far are summarised as below:

- Under the steady state condition, the pressure loss over the LBE-cooled reactor core is much lower than over the sodium-cooled cores.
- The sub-criticality of the present systems is large (over 4 USD). The effect of the feedback reactivity is too small to reduce the reactor power sufficiently to avoid the overheating of the coolant, the cladding and the fuel in unprotected transients.
- In the sodium-cooled systems, the transient behaviour in the unprotected loss-of-flow scenario shows the least favourable safety performance. Coolant boiling, cladding failure and molten fuel injection take place just in several seconds after the coast-down of the pump.
- In the LBE-cooled systems, a strong buoyancy driving force is obtained. By a proper design of the primary loop, the natural convection would provide a sufficiently high cooling capability of the reactor core. Overheating of the coolant, the cladding and the fuel can be avoided.

The results indicate clearly the necessity of designing a reliable safety system, especially in the sodium-cooled systems. Two possible approaches, to avoid coolant boiling and fuel pin failure, are: (a) to design an effective and powerful natural circulation system, so that the mass flow rate can be kept above a certain level under natural convection conditions, (b) to design a passive mechanism to reduce or to remove the external source, before the coolant temperature exceeds the design limit.

REFERENCES

[1] ADTF Design Team, private communication, Argonne National Laboratory, May 2001-January 2002.

[2] EBR-II System Design Description, Vol. I-V, ANL Internal Document, 15 June 1972.

[3] C.P. Cabell (1980), *A Summary Description of the Fast Flux Test Facility*, HEDL-400, Hanford Engineering Development Laboratory, December.

[4] L. Mercatali, private communication, Argonne National Laboratory, July 2001-March 2002.

[5] W.S. Yang, H. Khalil, private communication, Argonne National Laboratory, 2001.

[6] J. Stilman, private communication, Argonne National Laboratory, August 2001.

[7] X. Cheng (2002), *Safety Analysis of the Accelerator-driven Test Facility*, ANL-AAA-012, Argonne National Laboratory, May 2002.

[8] M. Eriksson, J. Cahalan (2001), *Applicability of Passive Safety to Accelerator-driven Systems*, AccApp/ADTTA'01, November 11-15, 2001, Reno, NV.